Intraoperative brain shift compensation using a hybrid mixture model

Siming Bayer[1], Nishant Ravikumar[1], Maddalena Strumia[2], Xiaoguang Tong[3],
Ying Gao[4], Martin Ostermeier[2], Rebecca Fahrig[2], and Andreas Maier[1]

[1] Pattern Recognition Lab, Friedrich-Alexander University, Martenstaße 3 91058
Erlangen, Germany
siming.bayer@fau.de
[2] Siemens Healthcare GmbH, Siemensstr. 1 91301 Forchheim, Germany
[3] Tianjin Huanhu Hospital, Jizhao Road 6 300350 Tianjin, China
[4] Siemens Healthcare Ltd, Wanjing Zhonghuan Nanlu 100102 Beijing, China

Abstract. Brain deformation (or *brain shift*) during neurosurgical pro-
cedures such as tumor resection has a significant impact on the accuracy
of neuronavigation systems. Compensating for this deformation during
surgery is essential for effective guidance. In this paper, we propose a
method for *brain shift* compensation based on registration of vessel cen-
terlines derived from preoperative C-Arm cone beam CT (CBCT) im-
ages, to intraoperative ones. A hybrid mixture model (HdMM)-based
non-rigid registration approach was formulated wherein, Student's t and
Watson distributions were combined to model positions and centerline
orientations of cerebral vasculature, respectively. Following registration
of the preoperative vessel centerlines to its intraoperative counterparts,
B-spline interpolation was used to generate a dense deformation field and
warp the preoperative image to each intraoperative image acquired. Reg-
istration accuracy was evaluated using both synthetic and clinical data.
The former comprised CBCT images, acquired using a deformable an-
thropomorphic brain phantom. The latter meanwhile, consisted of four
3D digital subtraction angiography (DSA) images of one patient, ac-
quired before, during and after surgical tumor resection. HdMM consis-
tently outperformed a state-of-the-art point matching method, coherent
point drift (CPD), resulting in significantly lower registration errors. For
clinical data, the registration error was reduced from 3.73mm using CPD
to 1.55mm using the proposed method.

1 Introduction

Brain shift compensation is imperative during neurosurgical procedures such as
tumor resection as the resulting deformation of brain parenchyma significantly
affects the efficacy of preoperative plans, central to surgical guidance. Conven-
tional image-guided navigation systems (IGNS) model the skull and its contents
as rigid objects and do not compensate for soft tissue deformation induced dur-
ing surgery. Consequently, non-rigid registration is essential to update surgical
plans, and ensure precision during image-guided neurosurgery.

C-arm computed tomography (CT) is a state-of-the-art imaging system, capable of acquiring high resolution and high contrast 3D images of cerebral vasculature in real time. However, in contrast to other intraoperative imaging systems such as magnetic resonance (MR), ultrasound (US), laser range scanners and stereo vision cameras, few studies have investigated the use of C-arm CT in an interventional setting for *brain shift* compensation [1]. The advantages of C-arm interventional imaging systems are, they do not require special surgical tools as with MR and provide high resolution images (unlike MR and US). Additionally, they enable recovery of soft tissue deformation within the brain, rather than just the external surface (as with laser range imaging and stereo vision cameras). The downsides are a slight increase in X-ray and contrast agent dose.

Recently, Smit-Ockeleon et al. [5] employed B-spline based elastic image registration to compensate for *brain shift*, using pre- and intraoperative CBCT images (although, not during surgical tumor resection). Coherent point drift (CPD) [8], a state-of-the-art non-rigid point set registration approach was used in [3] and [7], for *brain shift* compensation. Both studies used thin plate splines (TPS)-based interpolation to warp the preoperative image to its intraoperative counterparts, based on the initial sparse displacement field estimated using CPD. Although [3] demonstrated the superiority of CPD compared to conventional point matching approaches such as iterative closest point (ICP), a fundamental drawback of the former in an interventional setting is that it lacks automatic robustness to outliers. To overcome this limitation, Ravikumar et al. [10] proposed a probabilistic point set registration approach based on Student's t-distributions and Von-Mises-Fisher distributions for group-wise shape registration.

In this paper we propose a vessel centerlines-based registration framework for intraoperative *brain shift* compensation at different stages of neurosurgery, namely, at dura-opening, during tumor resection, and following tumor removal. The main contributions of our work are: (1) a feature based registration framework that enables the use of 3D digital subtraction angiography (DSA) images and 3D CBCT acquired using C-arm CT, for *brain shift* compensation; (2) the formulation of a probabilistic non-rigid registration approach, using a hybrid mixture model (HdMM) that combines Student's t-distributions ($\mathcal{S}$, for automatic robustness to outliers) to model spatial positions, and Watson distributions ($\mathcal{W}$) to model the orientation of vessel centerlines; and (3) to the best of our knowledge, this is the first paper exploring the use of pre-, intra-, and post-surgery 3D DSA for *brain shift* compensation in a real patient.

2   Material and Methods

This study investigates the use of C-Arm CT, which captures 3D cerebral vasculature, as pre- and intraoperative image modalities for *brain shift* compensation during surgical tumor resection. Vessel centerlines were extracted from pre- and intraoperative images automatically using Frangi's vesselness filter [4] and a homotopic thinning algorithm proposed in [6]. The registration pipeline we fol-

lowed is: 1) rigid and non-rigid registration, 2) an optional resection detection and registration refinement step, and 3) B-Spline image warping.

Hybrid mixture model-based registration: The extracted centerlines are represented as 6D hybrid point sets, comprising spatial positions and their associated undirected unit vectors representing the local orientation of vessels. Preoperative centerlines are registered to their intraoperative counterparts using a pair-wise, hybrid mixture model-based rigid and non-rigid registration approach. Rigid registration is used to initialize the subsequent non-rigid step, in all experiments conducted. Recently, [10] proposed a similar approach for group-wise shape registration. Here, hybrid shape representations which combined spatial positions and their associated (consistently oriented) surface normal vectors are employed to improve registration accuracy for complex geometries. However, their approach is designed to model directional data using Von-Mises-Fisher (vmF) distributions and correspondingly required the surface normal vectors to be consistently oriented. vmF distributions lack antipodal symmetry and consequently are not suitable to model axial data such as vessel centerlines. We propose a variant of this registration approach that incorporates Watson distributions (whose probability density is the same in either direction along its mean axis) in place of vmFs, to address this limitation.

Registration of the preoperative (`Source`) and intraoperative (`Target`) vessel centerlines is formulated as a probability density estimation problem. Hybrid points defining the `Source` are regarded as the centroids of a HdMM, which is fit to those defining the `Target`, regarded as its data points. This is achieved by maximizing the log-likelihood (*llh*) function, using expectation-maximization (EM). The desired rigid and non-rigid transformations are estimated during the maximization (M)-step of the algorithm. By assuming the spatial position ($\mathbf{x}_i$) and centerline orientation ($\mathbf{n}_i$) components of each hybrid point in the `Target` set to be conditionally independent, their joint probability density function (PDF) can be approximated as a product of the individual conditional densities. The PDF of an undirected 3D unit vector $\mathbf{n}_i$ sampled from the jth component's Watson distribution in a HdMM, with a mean $\mathbf{m}_j$, is expressed as: $p(\pm\mathbf{n}_i|\mathbf{m}_j, \kappa_j) = M(\frac{1}{2}, \frac{D}{2}, \kappa_j)^{-1} \exp^{\kappa_j (\mathbf{m}_j{}^T \mathbf{n}_i)^2}$. Here, κ_j and $M(\cdot)$ represent the dispersion parameters and confluent hypergeometric function, respectively.

$$\log(\mathbf{T} \mid \mathcal{T}, \Theta_p, \Theta_d) = \sum_{i=1}^{N} \log \sum_{j=1}^{M} \pi_j \mathcal{S}(\mathbf{x}_i \mid \mathcal{T}\boldsymbol{\mu}_j, \nu_j, \sigma^2) \mathcal{W}(\mathbf{n}_i \mid \mathcal{T}\mathbf{m}_j, \kappa_j) \quad (1a)$$

$$Q(\Theta_p^{t+1} \mid \Theta_p^t) = \sum_{i,j=1}^{N,M} -P_{i,j}^{\star} \frac{||\mathbf{x}_i - (\boldsymbol{\mu}_j + v(\boldsymbol{\mu}_j))||^2}{2\sigma^2} + \frac{\lambda}{2} \operatorname{Tr}\{\mathbf{W}^T \mathbf{G} \mathbf{W}\} \quad (1b)$$

Assuming all $i = 1...N$ hybrid points in the `Target` ($\mathbf{T}$) to be independent and identically distributed, and as data points generated by an $j = 1...M$-component mixture model (defining the `Source`), the *llh* is expressed as shown in eq. 1a. Here, $\boldsymbol{\mu}_j$ and π_j represent the spatial position and mixture coefficient of the jth component in the HdMM. In the first stage, rigid transformation ($\mathcal{T}$) and

model parameters associated with the Student's t-distributions in the mixture ($\Theta_p = \{\nu_j, \sigma^2\}$), namely, translation, rotation, scaling, and degrees of freedom (ν_j), variance (σ^2), respectively, are updated in the M-step similarly to [9]. In the second stage, the desired non-rigid transformation ($\mathcal{T}$) is expressed as a linear combination of radial basis functions, and the associated parameters are estimated as described in [8]. Tikhonov regularization is employed to ensure that the estimated deformation field is smooth. The resulting cost function that is maximized to estimate the desired non-rigid transformation is expressed as shown in eq. 1b. Here, Q represents the expected *llh*, t represents the current EM-iteration, $P^\star$ represents the corrected posterior probabilities estimated in the expectation (E)-step (as described in [9]), v is the displacement function mapping the `Source` to the `Target`, λ controls the smoothness enforced on the deformation field and $\mathbf{W}$ and $\mathbf{G}$ represent the weights associated with the radial basis functions and the Gaussian kernel, respectively. During both rigid and non-rigid registration, parameters associated with the Watson distributions ($\Theta_d = \{\kappa_j\}$) are estimated as described in [2].

Resection detection and registration refinement: While the Student's t-distributions in the proposed framework provide automatic robustness to outliers, it is difficult to cope with large amounts of missing data in the `Target` relative to the `Source`, as is the case during and following tumor resection. Consequently, we formulated a mechanism for refining the correspondences, in order to accommodate for the missing data during registration. This was achieved by detecting and excluding points in the `Source` that lie within the resected region in the `Target`, following both rigid and non-rigid registration. The refined correspondences in the `Source` were subsequently non-rigidly registered (henceforth referred to as HdMM+) to the `Target`, to accommodate for the missing data and improve the overall registration accuracy. Points within the resected region were identified by first building a 2D feature space for each point in the `Source`. The selected features comprised: the minimum euclidean distance between each `Source` point and the points in the `Target`; and the number of points in the `Target` which had been assigned posterior probabilities greater than $1e^{-5}$, for each point in the `Source`. Subsequently, PCA was used to reduce the dimensionality of this feature space and extract the first principal component. Finally, automatic histogram clipping using Otsu-thresholding was performed on the first principal component, to identify and exclude points within the resected region.

3 Experiments and Results

Data acquisition: A deformable anthropomorphic brain phantom Fig. 1, (manufactured by True Phantom Solutions Inc., Windsor, Canada) is used to acquire CBCT images and conduct synthetic experiments. It comprises multiple structures mimicking real anatomy, namely, skin, skull, brain parenchyma, ventricular system, cerebral vasculature and an inflatable tumor. A removable plug is embedded in the skull to emulate a craniotomy. Brain tissue and blood vessels are made from polyurethane, a soft tissue simulant. In order to simulate mul-

tiple stages of tumor resection surgery, 40ml distilled water was injected into the inflatable tumor initially. The tumor was subsequently deflated to 25ml, 15ml, 5ml and 0ml. At each stage, a 10s 3D CBCT image was acquired using the Ultravist 370 contrast agent to enhance the blood vessels. The acquisitions were reconstructed on a 512x512x398 grid at a voxel resolution of $0.48mm^3$. The experimental setup and a typical acquisition of the phantom are shown in Fig. 1. A detailed description and visualization of the phantom is included in the supplementary material.

The clinical data used in this study was provided by our clinical partner. It comprised 3D DSA images acquired during tumor resection surgery of a glioma patient. The images were acquired preoperatively, following craniotomy, during resection, and postoperatively, to monitor blood flow within the brain during and after surgery. The surgery was performed in a hybrid operating room with Siemens Artis zeego system (Forchheim, Germany) and as with the phantom experiments, the acquisitions were reconstructed on a 512x512x398 grid with voxel resolution of $0.48mm^3$. We evaluated the proposed approach using the phantom

Fig. 1. The CAD model of the phantom, the experiment setting and an example slice of CBCT acquisition of the phantom are shown from left to right.

and clinical data sets. The former involved four independent registration experiments. The image acquired with the tumor in its deflated state (with 0ml of water) was considered to be the `Source`, while, those acquired at each inflated state of the tumor were considered as `Targets`. The latter involved three independent experiments, namely, registration of the preoperative image to images acquired following craniotomy, during tumor resection, and postoperatively.

Results: We compared the performance of our registration method with CPD, using the phantom and clinical data sets. For fair comparison, we fixed the parameters associated with the non-rigid transformation, namely, the smoothing factor associated with the Tikhonov regularization and the width of the Gaussian kernel, to 1, for both HdMM and CPD. Following preliminary investigations, we identified 0.5 to be a suitable value for the uniform distribution component weight in CPD, which remained fixed for all experiments. The maximum number of EM-iterations was set to 100 for all experiments, using both methods. The mean surface distance metric (MSD) is used to evaluate registration accuracy in all experiments conducted. As the phantom data set lacks any tumor resec-

tion/missing data, these samples are registered using just CPD and HdMM. In contrast, the clinical data set is registered using CPD, HdMM and HdMM+, to evaluate the gain in registration accuracy provided by the correspondence refinement step (in HdMM+), when dealing with missing data. We assess registration accuracy for both data sets in two ways: (1) by evaluating the MSD between the registered `Source` and `Target` sets (henceforth referred to as `Error1`); and (2) by evaluating the MSD between the vessel centerlines, extracted from the warped preoperative image, and each corresponding intraoperative image (henceforth referred to as `Error2`). Additionally, for the clinical data set, in order to evaluate the degree of overlap between the cerebral vasculature following registration of the preoperative to each intraoperative image, we also compute the Dice and Jaccard scores between their respective vessel segmentations.

The average MSD errors, Dice, and Jaccard scores for all experiments are summarized by the box plots depicted in Fig. 2. These plots indicate that, HdMM consistently outperforms CPD in all experiments conducted, and in terms of all measures used to assess registration accuracy. The initial average MSD is 5.42 ± 1.07mm and 6.06 ± 0.68mm for phantom and clinical data, respectively. Applying the registration pipeline, the average `Error1` for the phantom data set (averaged across all four registration experiments), is 0.89 ± 0.36mm and 0.50 ± 0.05mm, using CPD and HdMM respectively. While, the average `Error2` is 1.88 ± 0.52mm and 1.54 ± 0.15mm for CPD and HdMM, respectively. For the clinical data set, the average `Error1` is 2.44 ± 0.28mm and 1.15 ± 0.36mm and average `Error2` is 3.72 ± 0.46mm and 2.24 ± 0.55m, for CPD and HdMM, respectively. Further improvement in registration accuracy is achieved using HdMM+, which achieved average `Error1` and `Error2` of 0.78 ± 0.12mm and 1.55 ± 0.22mm, respectively. The mean Dice and Jaccard scores (refer to Fig.2(c)) evaluated using
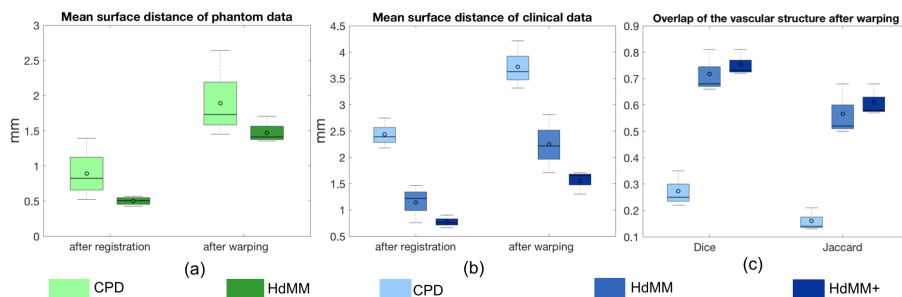

Fig. 2. MSD errors evaluated following registration of the phantom and clinical data sets are presented in (a) and (b) respectively. Average Dice and Jaccard scores evaluating the overlap between vessels segmented in the registered preoperative and corresponding intraoperative images are depicted in (c).

vessels segmented from the warped preoperative image and each corresponding intraoperative image indicate that, similar to the MSD errors, HdMM+ outper-
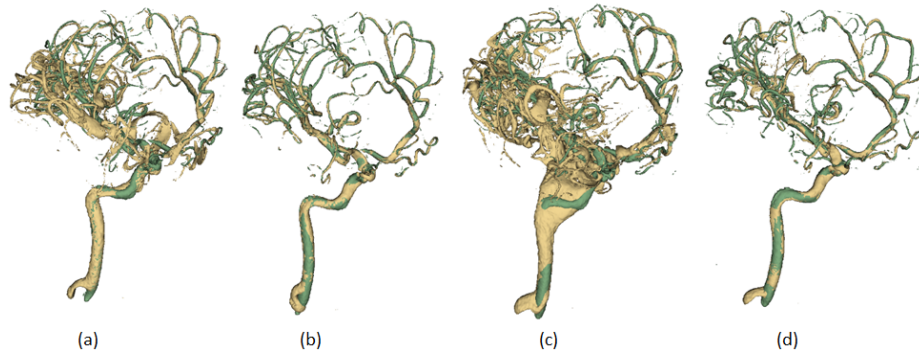
Fig. 3. Overlay of 3D cerebral vasculature segmented from the registered preoperative (yellow) DSA image and the target intraoperative image (green). Using CPD (a) and HdMM (b) prior to resection, using CPD (c) and HdMM (d) post resection.

formed both CPD and HdMM. To qualitatively assess the registration accuracy of our approach, vessels extracted from the warped preoperative image, are overlaid on its intraoperative counterpart (acquired following craniotomoy and tumor resection), as shown in Fig. 3. Fig. 3(a) and (c) depicts the registration result of CPD, while, Fig. 3(b) and (d) depicts that of HdMM. These images summarize the superior registration accuracy of the proposed approach, relative to CPD.

4 Discussion and Conclusion

The presented results (refer to Fig. 2 - 3) for the phantom and clinical data experiments indicate that the proposed approach is able to preserve fine structural details, and consistently outperforms CPD in terms of registration accuracy. This is attributed to the higher discriminative capacity afforded by the hybrid representation of vessel centerlines used by HdMM, enabling it to establish correspondences with greater anatomical validity than CPD. Complex structures such as vessel bifurcations require more descriptive features for accurate registration, than afforded by spatial positions alone. Consequently, a registration framework such as HdMM that jointly models the PDF of spatial positions and centerline orientations, is better equipped for registering complex geometries such as cerebral vasculature than point matching methods that rely on spatial positions alone (such as CPD).

An additional advantage of the proposed approach is its inherent and automatic robustness to outliers that may be present in the data. This is attributed to the heavy-tailed nature of the constituent Student's t-distributions in the HdMM, and the estimation of different values for the degrees of freedom associated with each component in the HdMM. This is a significant advantage over CPD, as the latter requires manual tuning of a weight associated with the uniform distribution component in the mixture model, which regulates its robustness to outliers during registration. These advantages and the significant

improvement in registration accuracy afforded by HdMM indicate that it is well-suited to applications involving registration of vascular structures. This is encouraging for its future use in intraoperative guidance applications, and specifically, for vessel-guided *brain shift* compensation.

Evaluation on a single clinical data set is a limitation of the current study. However, the proposed work-flow is not standard clinical practice, as there is a limited number of hybrid installations, equipped with CBCT capable devices in upright sitting position. Furthermore, the protocol induces a slight amount of additional X-ray and contrast agent dose which is typically not a problem for the patient population under consideration. However, prior to this study, there was no indication whether vessel-based *brain shift* compensation can be performed successfully at all, given 3D DSA images. Thus, getting a single data set posed a significant challenge. The potential of the proposed workflow to ensure high precision in surgical guidance, in the vicinity of cerebral vasculature, is particularly compelling for neurosurgery.

Disclaimer: The methods and information presented in this work are based on research and are not commercially available.

References

1. Bayer, S., Maier, A., Ostermeier, M., Fahrig, R.: Intraoperative Imaging Modalities and Compensation for Brain Shift in Tumor Resection Surgery. Int. J. Biomed. Imaging (2017)
2. Bijral, A., Breitenbach, M., Grudic, G.: Mixture of watson distributions: a generative model for hyperspherical embeddings. In: Proceedings of Machine Learning Research (2007)
3. Farnia, P., Ahmadian, A., Khoshnevisan, A., Jaberzadeh, A., Serej, N.D., Kazerooni, A.F.: An efficient point based registration of intra-operative ultrasound images with mr images for computation of brain shift; a phantom study. In: IEEE EMBC 2011. pp. 8074-8077 (2011)
4. Frangi, A.F., Niessen, W.J., Vincken, K.L., Viergever, M.A.: Multiscale vessel enhancement filtering. In: MICCAI 1998. pp. 130-137 (1998)
5. Iris Smit-Ockeloen, Daniel Ruijters, Marcel Breeuwer, Drazenko Babic, Olivier Brina, Pereira, V.M.: Accuracy Assessment of CBCT-Based Volumetric Brain Shift Field. In: Lecture Notes in Computer Science. vol. 9401, pp. 1-9 (2016)
6. Lee, T., Kashyap, R., Chu, C.: Building skeleton models via 3-d medial surface axis thinning algorithms. CVGIP 56(6), 462-478 (1994)
7. Marreiros, F.M.M., Rossitti, S., Wang, C., Smedby, Ö.: Non-rigid Deformation Pipeline for Compensation of Superficial Brain Shift. In: MICCAI 2013. pp. 141-148 (2013)
8. Myronenko, A., Song, X.: Point set registration: Coherent point drift. IEEE Trans. Pattern. Anal. Mach. Intell. 32(12), 2262-2275 (2010)
9. Ravikumar, N., Gooya, A., Çimen, S., Frangi, A.F., Taylor, Z.A.: Group-wise similarity registration of point sets using students t-mixture model for statistical shape models. Med. Image. Anal. 44, 156-176 (2018)
10. Ravikumar, N., Gooya, A., Frangi, A.F., Taylor, Z.A.: Generalised Coherent Point Drift for Group-Wise Registration of Multi-dimensional Point Sets. In: MICCAI 2017. pp. 309-316 (2017)